The enhanced chemotherapeutic effects of doxorubicin loaded PEG coated TiO_2 nanocarriers in an orthotopic breast tumor bearing mouse model†

Yang Du,‡[a] Wenzhi Ren,‡[b] Yaqian Li,[ac] Qian Zhang,[a] Leyong Zeng,[b] Chongwei Chi,[a] Aiguo Wu*[b] and Jie Tian*[a]

Many chemotherapeutics used for cancer treatments encounter issues during delivery to tumors *in vivo* and have high levels of systemic toxicity. One of the most prominent progresses in improving drug delivery efficiency is through exploring various types of nanoparticles (NPs) as drug carriers. Recent studies have demonstrated that titanium dioxide (TiO_2) nanocarriers have potential for drug delivery and therapy even in multidrug resistant cancers *in vitro*. Moreover, it was proved that the anticancer activity of doxorubicin (DOX) was enhanced by loading onto TiO_2 nanoparticles in breast cancer cells *in vitro*. However, there is no evidence from the animal model *in vivo*, which is a critical step for their further clinical applications. The aim of this study was to explore novel TiO_2–PEG–DOX nanoparticles, the DOX loaded polyethylene glycol (PEG) coated TiO_2 nanocarriers, and investigate their potential application in enabling controlled drug release and enhancing the chemotherapeutic efficacy of DOX in the orthotopic breast tumor bearing mice. The tumor growth and drug treatment efficacy were dynamically monitored by bioluminescence imaging (BLI), and the safety of NPs for *in vivo* usage was also evaluated. It was found that TiO_2–PEG–DOX nanoparticles possessed improved antitumor efficacy without observable side effects compared to the free DOX treatment. Our study suggested that the PEG coated TiO_2 nanocarrier is a safe and potential platform for the efficient drug delivery and minimizing the systemic toxicity of chemotherapeutic agents. It has been proved for the first time that TiO_2-based nanocarriers enhance the chemotherapeutic effects of doxorubicin *in vivo*.

1. Introduction

Breast cancer is one of the leading causes of cancer morbidity and mortality among women worldwide, and the frequency keeps increasing.[1–3] Chemotherapy is a major clinical approach for cancer treatment by using cytotoxic antitumor drugs. Traditional chemotherapeutics are usually nonspecifically distributed in the whole body through blood circulation, which may cause systemic side effects. The poor specificity and limited accumulation of anticancer drugs in tumor regions cause various adverse side effects, such as myelosuppression, gastrointestinal distress, alopecia, organ damage, *etc.* These effects can cause pain in patients and eventually the failure of therapy.[4,5] The use of various pharmaceutical nanocarriers has become one of the most important areas of nanomedicine. Ideally, such carriers can be specifically delivered to the pathological areas to provide the maximum therapeutic efficacy. Therefore, it prompted scientists to explore the feasibility of developing nanoparticles as effective drug delivery vehicles to overcome the limited therapeutic efficacy of free drugs and circumvent their toxicity.

The prominent progress of nanomedicine is through the continuous development of nanoparticle (NP)-based therapy, which exhibited the potential for unparalleled performance over conventional tools.[6,7] The development of nanotechnology driven drug delivery holds the potential for revolutionizing cancer chemotherapy.[8] By controlling the nanoparticle size, the drug delivery efficacy to the tumor sites can be greatly increased through the enhanced permeability and retention (EPR) effect, which is due to tumor vasculature abnormalities and reduces the drug's cytotoxicity simultaneously.[9] Particularly, inorganic

[a]*Key Laboratory of Molecular Imaging, The State Key Laboratory of Management and Control for Complex Systems, Institute of Automation, Chinese Academy of Sciences, 95 ZhongGuanCun East Road, 100190, Beijing, China. E-mail: jaytian99@gmail.com*

[b]*Key Laboratory of Magnetic Materials and Devices & Division of Functional Materials and Nanodevices, Ningbo Institute of Materials Technology and Engineering, Chinese Academy of Sciences, 1219 ZhongGuan West Road, 315201, Ningbo, China. E-mail: aiguo@nimte.ac.cn*

[c]*Harbin University of Science and Technology, Harbin, China*

† Electronic supplementary information (ESI) available. See DOI: 10.1039/c4tb01781a

‡ Yang Du and Wenzhi Ren contributed equally to the present paper.

NPs have received great attention due to their outstanding properties. Inorganic NPs can be designed to enhance the accumulation of drugs at the tumor sites when administered *in vivo*. The unique size scale of inorganic NPs can enable their preferential accumulation in the tumor region through EPR effects.[10] A variety of inorganic nanocarriers, such as iron oxide, mesoporous silica, graphene oxide and titanium dioxide nanoparticles, have been studied for successful drug delivery and therapy in cancer treatment.[11–16] Furthermore, metal nanomaterials have also been widely studied as drug carriers, which represent a promising approach to tumors.[17,18] The titanium dioxide (TiO_2) nanoparticle possesses many attractive features such as excellent biocompatibility, low toxicity, high chemical stability, and unique photocatalytic and sonocatalytic properties. Therefore, it has received much attention in the field of photodynamic therapy and sonodynamic therapy of cancer, even in the field of potential multimodal therapy agents.[19] Based on its unique properties, the TiO_2 nanoparticle also draws much attention in the field of drug delivery of chemotherapeutic drugs.[20–24] For example, Yan Chen *et al.* constructed a DOX–TiO_2 nanoparticle as a drug delivery system, and the results showed that the anti-cancer efficacy of the drug per dose dramatically increased in human SMMC-7721 hepatocarcinoma cells.[25] It was found that Fe_3O_4@TiO_2 core–shell nanocomposites with 6–8 nm diameter have been explored as carriers for DOX delivery in drug-resistant ovarian carcinoma cells.[16] In addition, Wenzhi Ren *et al.* reported an enhanced doxorubicin transport to multidrug resistant breast cancer cells *via* TiO_2 nanocarriers.[26]

However until now, there has been no report on the application of TiO_2-based nanocarriers in the animal model, which is a critical step to learn how they behave *in vivo* for their further clinical applications. Therefore, novel TiO_2–PEG–DOX nanoparticles were constructed and characterized in this study, and it is hypothesized that TiO_2–PEG–DOX NPs were able to increase the specific targeting of DOX at the tumor site *in vivo*, increasing treatment efficacy and reducing the nonspecific toxicity to other organs. Polyethylene glycol (PEG) was coated onto TiO_2 with the purpose of improving the stability of TiO_2–DOX NPs. It is also known that most nanomaterials, when administered into the blood, are taken up by phagocytic cells of the mononuclear phagocyte system (MPS) in the liver and spleen within minutes or hours. The addition of PEG to the surface of nanomaterials can avoid their rapid clearance by the MPS. By preventing opsonization, the addition of PEG greatly increases the blood half-life of all nanomaterials and therefore enhances the accumulation of nanomaterials in tumor tissue.[27–29]

In this study, we investigate the potential application of TiO_2–PEG–DOX NPs in enabling controlled drug release and enhancing the chemotherapeutic efficacy of DOX in the orthotopic breast tumor bearing mice. In order to fully monitor tumor growth and examine drug treatment effects in a sensitive way, bioluminescence imaging (BLI) was performed on the orthotopic breast tumor-bearing mice during the whole 15 day treatment. Optical molecular imaging, such as BLI, has several advantages over traditional methods, especially in the field of *in vivo* cancer research. It enables sensitive and longitudinal observation and has become an important tool for early lesion detection and monitoring therapeutic efficacy.[30,31] The firefly luciferase labeled MDA-MB-231-GFP-fLuc breast cancer cell line was used in our study to establish the breast tumor animal model for *in vivo* experiments. Moreover, the H&E histology and CD31 immunostaining of tumors and major organs were performed at the end of experiments to further evaluate the antitumor efficacy and the toxicity of different treatments.

2. Materials and methods

2.1 Materials

Doxorubicin (DOX) was obtained from Ningbo Hangjing biotechnology Co. Ltd. (Ningbo, China). D-Luciferin reagent was purchased from Biotium (CA, Fremont, USA). Fetal calf serum was purchased from HyClone (Thermo Scientific, US). All other reagents were of analytical grade. The breast cancer cell line MDA-MB-231-GFP-fLuc cells were kindly provided by the Department of Radiology, Peking Union Medical College Hospital.

2.2 Preparation of TiO_2–PEG–DOX nanoparticles

Nanoparticles (TiO_2 NPs) were prepared by our reported method with modification.[26] Briefly, $TiCl_4$ was hydrolyzed and dialyzed in water, and then heated to improve the crystallinity of TiO_2 NPs. The concentration of as-prepared TiO_2 NPs was 0.5 mg mL^{-1} which was determined by ICP-MS (NexION 300, Perkin-Elmer, US). In order to improve the stability of TiO_2 NPs, polyethylene glycol (PEG, molecular weight 1500) was used to enwrap the nanoparticles. 20 mL of TiO_2 NPs (0.5 mg mL^{-1}) were dropped into PEG solution, and stirred for 24 h. TiO_2–PEG NPs were separated by centrifugation at 12 500 rpm for 30 min, and were dispersed in 20 mL ultrapure water. 1 mL of DOX (1 mg mL^{-1}) were drop-wise added into TiO_2–PEG NPs and stirred for another 24 h. The obtained TiO_2–PEG–DOX NPs were collected by centrifugation at 12 500 rpm for 30 min and stored at 4 °C. Furthermore, free DOX in the centrifugal supernatant was also collected to measure the loading efficiency of DOX onto TiO_2–PEG. The absorption of DOX (0–1 mg mL^{-1}) at 488 nm was determined using a UV-visible spectrophotometer. The dose–absorption curve of DOX was calculated according to the different absorptions of DOX at 488 nm. The collected free DOX was determined using a UV visible spectrophotometer, and the concentration of the free DOX was calculated by the dose–absorption curve of DOX. The loading efficiency of DOX onto TiO_2–PEG = (total DOX − free DOX) ÷ (amount of TiO_2) × 100% = (1 mg mL^{-1} × 1 mL–0.0056 mg mL^{-1} × 21 mL) ÷ (0.5 mg mL^{-1} × 20 mL) × 100% = 8.82% (Fig. 1).

2.3 Characterization of TiO_2–PEG–DOX NPs

In order to investigate the hydrated particle size and stability of the nanoparticles, TiO_2–PEG or TiO_2–PEG–DOX NPs were dispersed in fetal bovine serum for 7 days at room temperature, the size of the nanoparticles was measured every day using a particle size-zeta potential analyzer (Nano ZS, Malvern Instruments Ltd, England). The UV-visible absorption of TiO_2–PEG

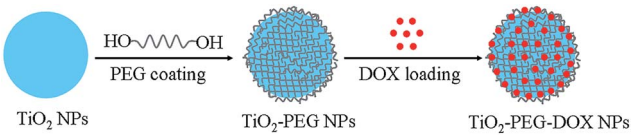

Fig. 1 The fabrication process of TiO_2–PEG–DOX NPs. First, TiO_2 NPs were coated with PEG to increase their stability, and then DOX was added into TiO_2–PEG NPs to form the TiO_2–PEG–DOX NPs.

NPs, TiO_2–PEG–DOX NPs and DOX was determined using a UV-visible spectrophotometer (T10CS, Beijing Purkinje General Instrument, China). The zeta potential of the nanoparticles was analyzed using a particle size-zeta potential analyzer.

For analysis of drug release, 2 mL TiO_2–PEG–DOX NPs containing 275 μg mL^{-1} DOX and 3118 μg mL^{-1} TiO_2 were equally transferred into two dialysis bags. The dialysis bags were respectively immersed into 24 mL buffer solution whose pH value was 7.4 or 5.0. The dialysis solution was collected at the scheduled time, and replaced with the same fresh buffer solution. The absorption of released DOX was then measured using a UV-visible spectrophotometer; the amount of the released DOX was calculated according to the dose–absorption curve of DOX.

2.4 MDA-MB-231-GFP-fLuc cell culture

MDA-MB-231-GFP-fLuc cells were cultured in Dulbecco's Modified Eagle Medium (DMEM, HyClone, Thermo Scientific, US) and supplemented with 10% fetal calf serum (FCS) (HyClone, Thermo Scientific, US). The cells were maintained in a 37 °C incubator with 5% CO_2.

2.5 Intracellular localization of DOX

The MDA-MB-231-GFP-fLuc breast cancer cells (1×10^5 cells per mL) were seeded into 35 mm culture dishes and cultured overnight. On the following day, the culture media were replaced by fresh medium with different treatments including control, TiO_2–PEG NPs, free DOX and TiO_2–PEG–DOX NPs containing 10 μg mL^{-1} DOX and 113 μg mL^{-1} TiO_2. The cells were incubated with TiO_2–PEG NPs for 2 h, free DOX and TiO_2–PEG–DOX NPs for 2 and 4 h, respectively. After incubation, the cells were washed with PBS and fixed with 4% formaldehyde for 30 min. The cells were washed with PBS after the nuclei were stained with Hoechst 33342 for 15 min. The intracellular localization of DOX was examined under a confocal microscope (TCS SP5, Leica Microsystems, Germany).

2.6 Cell viability assay

The MDA-MB-231-GFP-fLuc cells were plated in 96-well plates (1×10^4 cells per well) and cultured for 24 h. The cells were incubated with different doses of TiO_2–PEG NPs, free DOX or TiO_2–PEG–DOX NPs for 24, 48 and 72 h. The concentration of free DOX (0–10 μg mL^{-1}) was equal to the concentration of DOX in TiO_2–PEG–DOX NPs. The dose of TiO_2–PEG NPs (0–113 μg mL^{-1}) was the same as that of TiO_2 in TiO_2–PEG–DOX NPs. The viability of cells with different treatments was assayed by the MTT assay. Briefly, 10 μL MTT (5 mg mL^{-1}) reagent was added into each well and incubated for 4 h. Then DMSO was used to dissolve the formazan crystals. The absorbance was measured using a Microplate Absorbance Reader (Biorad iMARK™, USA).

2.7 Establishment of the MDA-MB-231-GFP-fLuc orthotopic tumor bearing mice model

4–5 week old athymic male Balb/c nude mice ($n = 20$) were purchased from the Department of Experimental Animals, Peking University Health Science Center. All animal experiments were performed in accordance with the guidelines of the Institutional Animal Care and Use Committee (IACUC) at Peking University (permit number: 2011-0039). Briefly, the orthotopic tumor model was established by injecting 100 μL MDA-MB-231-GFP-fLuc cell suspension (1×10^6 cells per mL) into the lower right mammary fat pad of the Balb/c nude mice.

2.8 Drug administration

The mice with a similar tumor volume of 80–100 mm^3 were randomly divided into 4 groups (5 mice per group) after tumor cell inoculation. The TiO_2, free DOX and TiO_2–PEG–DOX NP treatment were given *via* tail vein injection. The doxorubicin dosage in free DOX treatment was 4 mg kg^{-1} and was administered every 3 days during the 15 day treatment period. The amount of TiO_2 (45 mg kg^{-1}) was equivalent to that used for the TiO_2–PEG–DOX NP groups. The control group received an equal volume of 0.9% saline.

2.9 Mouse body weight and tumor volume measurement

The mice body weight was measured using an electronic balance every 3 days. The tumor volume was measured by using a digital caliper and calculated according to the formula $\pi \times L \times W^2/6$. L and W were the respective length and width of the tumor.

2.10 *In vivo* BLI of the orthotopic breast tumor model

BLI was performed on the orthotopic breast tumor bearing mouse model using a small animal optical molecular imaging system (IVIS Imaging Spectrum System) and analyzed using IVIS Living Imaging 3.0 software (PerkinElmer, USA) on day 0, 3, 6, 9, 12 and 15 during drug treatment. The mice were fasted overnight before the experiment to prevent food from interfering with imaging results. The mice were anesthetized with 2% isoflurane and received intraperitoneal injection of 80 μL D-luciferin solution (40 mg mL^{-1}) 10 min before BLI was started. The mice were kept in the supine position. The parameters for the BLI imaging system were binning = 4 and exposure time = 1 s.

2.11 Histology of major organs and tumor tissues after different treatments

Hematoxylin and eosin staining (HE staining) were performed for histological evaluation of major organs and tumor tissues after different drug treatments. The cryosections were rinsed with distilled water and stained with hematoxylin, followed by

rinsing with running tap water. After differentiation in 0.3% acid alcohol and another rinse, the sections were stained with eosin for 2 min. Finally, the sections were consecutively dehydrated, cleared and mounted, and were examined under an optical microscope (Leica, DMI3000).

2.12 Immunofluorescence staining of CD31 on tumor tissues after drug treatment

The tumor tissues were dissected out and frozen in the optimum cutting temperature (OCT) compound (Leica, Germany) after drug treatment. The tumors were cryosectioned (Leica CM1950, Germany) for 10 μm thickness and all the slides were stored in a −80 °C freezer before staining. The sections were fixed in acetone for 10 min and stained with the primary antibody of rat anti-mouse CD31 (BD Biosciences, USA) overnight at 4 °C. Donkey anti-rat Alexa Fluor® 488 (Invitrogen, USA) was stained as the secondary antibody for 2 h at room temperature. Negative control was performed with omitting the primary antibody and incubated with secondary antibody only. The sections were washed twice and mounted with mounting medium containing DAPI (Vector Laboratories, US).

2.13 Serum IFN-α ELISA assay

The effect of TiO_2–PEG NPs on the plasma IFN-α level was tested. Briefly, the 5–6 week old female Balb/c mice were injected with TiO_2–PEG NPs (45 mg kg^{-1}) or an equal volume of saline, intravenously. Plasma samples were collected 6 h post-injection, and the IFN-α level was analyzed using an IFN-α ELISA kit (R&D systems, USA).

2.14 Statistical analysis

The data were presented as the average of three independent experiments. One-way analysis of variance (ANOVA) or Student's *t*-test was used to determine the statistical differences. (*) P values <0.05 and (**) P values <0.01 were considered as statistically significant. Statistical analysis was performed by using Prism4.0 (San Diego, CA, USA).

3. Results and discussion

3.1 Characteristics of TiO_2–PEG–DOX NPs

Present authors' previous work had already shown that TiO_2–DOX NPs can increase the antitumor cell effects in multidrug resistant breast cancer cells *in vitro*.[26] However there is no evidence about the antitumor effects of TiO_2–DOX NPs *in vivo*. Therefore, based on previous work, we further created novel TiO_2–PEG–DOX NPs, which were modified with polyethylene glycol (PEG) coating onto the TiO_2 NPs (Fig. 1), and tested this new nanosystem on the orthotopic breast tumor mouse model *in vivo*, which is necessary for the clinical translation of the NPs in the future. The addition of PEG to the surface of nanomaterials can avoid the rapid clearance by renal and reticuloendothelial systems (RESs), and greatly increases the blood half-life of all nanomaterials and therefore enhances the accumulation of nanomaterials in tumor tissue.[27–29] In addition, PEG coated TiO_2 NPs may decrease the interaction between DOX and TiO_2, therefore increasing drug release from nanocarriers in tumor regions.

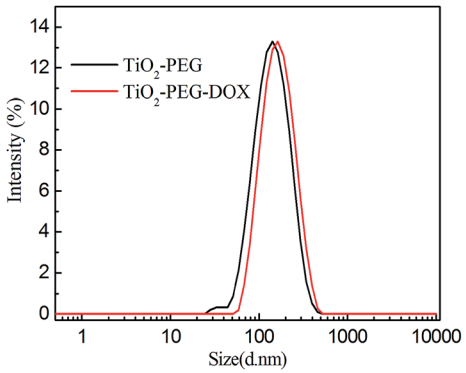

Fig. 2 Size distribution of TiO_2–PEG and TiO_2–PEG–DOX NPs.

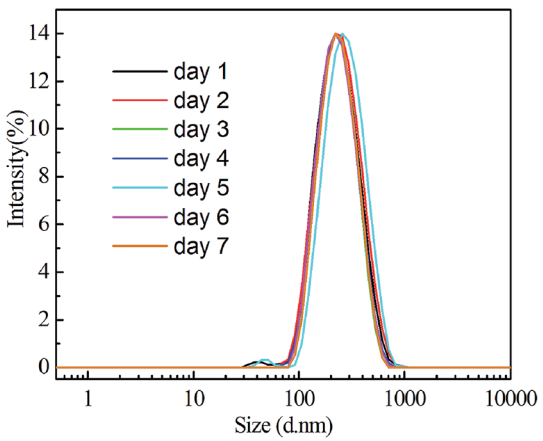

Fig. 3 Size distribution of TiO_2–PEG–DOX NPs in serum for continuous 7 days.

As shown in Fig. 2, the average hydrated diameter of TiO_2–PEG NPs was about 126 ± 2.6 nm. After loading with DOX, the hydrated size of TiO_2–PEG–DOX NPs was increased to 151 ±

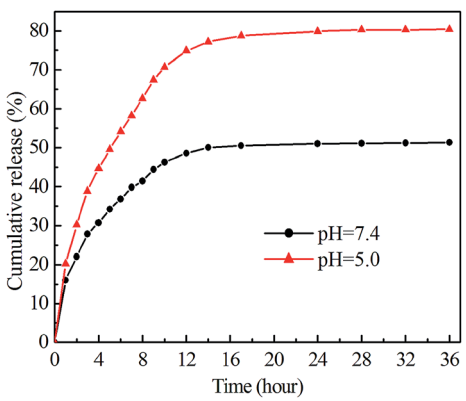

Fig. 4 pH controlled drug release of TiO_2–PEG–DOX NPs. The DOX release profiles at pH 7.4, and pH 5.0 are shown in black and red colored lines, respectively.

4.6 nm. The size of the NPs met the requirements of the EPR effect, which is favorable for the drug infiltration specifically at the tumor sites and correspondingly increase the chemotherapeutic efficacy. In addition, we further tested the stability of NPs, which is known to be critical to a successful drug delivery system. The results showed that the size of NPs did not show a great increase during 7 day culture in serum solution (Fig. 3), which suggested that TiO_2–PEG–DOX NPs were stable and can be administered intravenously *in vivo*.

The successful loading of DOX onto TiO_2–PEG NPs was confirmed by UV-visible spectra and zeta potential analysis. As shown in Fig. S1,† the characteristic peak of free DOX occurred at about 488 nm. Compared with TiO_2–PEG NPs, TiO_2–PEG–DOX NPs also possessed the peak of free DOX at around 488 nm, which suggested that DOX was adsorbed onto TiO_2–PEG NPs. Furthermore, zeta potential analysis also indicated that DOX was bound onto TiO_2–PEG NPs. As shown in Fig. S2,† owing to hydroxyl groups on the surface of TiO_2 NPs, the zeta potential of TiO_2–PEG NPs was −33.57 mV at a pH of 7.4. However, the zeta potential of TiO_2–PEG–DOX NPs was −26.27 mV at the same pH value, which was due to the positive charges of amino groups in the DOX neutralized part of negative charges on the TiO_2–PEG NP surface. In addition, it has been considered that negatively charged nanocarriers exhibited resistance to

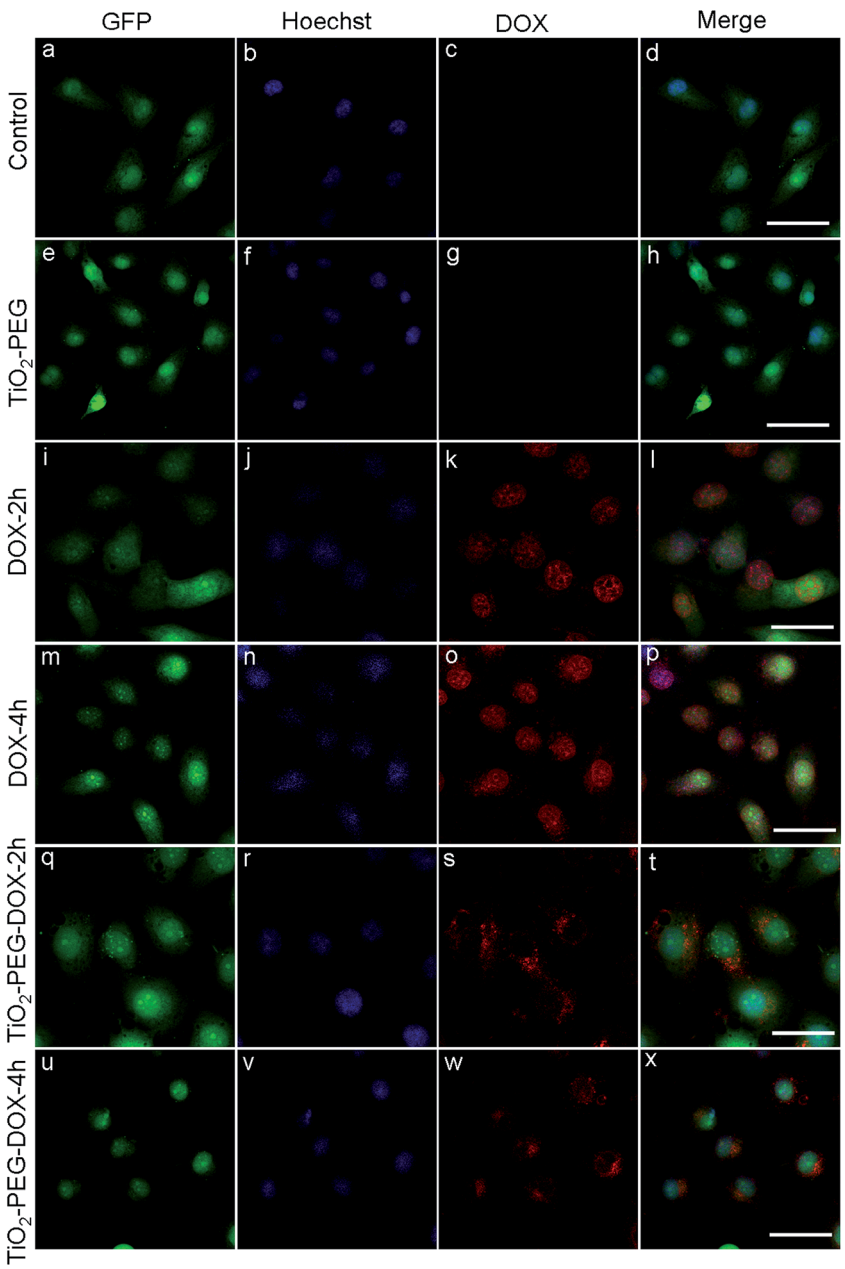

Fig. 5 Confocal microscopy images of the intracellular distribution of DOX in the MDA-MB-231-GFP-fLuc breast cancer cells. Control group is shown in (a–d); TiO_2–PEG NP treatment of cells is shown in (e–h). (i–l) and (m–p) show the cells incubated with DOX for 2 and 4 h, respectively. (q–t) and (u–x) show the cells incubated with TiO_2–PEG–DOX NPs for 2 and 4 h, respectively (scale bar = 50 μm, 40×).

adsorption of serum proteins, and therefore showed prolonged circulation time in blood which could enhance the accumulation of drugs in the tumor site.

3.2 Controlled drug release from TiO_2–PEG–DOX NPs *in vitro*

Controlled release capabilities are critical for drug delivery nanocarriers, and the pH responsiveness is one of the most frequently used biological stimuli exploited for the triggered drug release. Lactic acid is usually generated due to hypoxia and acidic intracellular organelles inside tumors, lowering the pH values dramatically in tumor regions relative to normal areas, therefore the pH values vary in the different biological compartments and the cellular organelles. These conditions may affect the interaction of drug and TiO_2 nanocarriers and facilitate drug release.[32,33] Our previous work suggested that the negatively charged TiO_2 surface could be turned into positive in an acidic environment, which attenuated the interactions between TiO_2 and DOX enhancing the drug release. However, a previous report also suggested that due to the bare TiO_2 NPs without any surface modification, the adsorption between TiO_2 and DOX was very strong. Therefore, only a part of the drug could be released even in the acidic environment of pH 5.0.[26] In this work, to further weaken the interaction between TiO_2 and DOX, and meanwhile, to increase the stability and blood half-life of the nanocarriers, PEG was used to coat TiO_2 NPs to form TiO_2–PEG NPs. Therefore, in this study, the DOX release from TiO_2–PEG–DOX NPs was evaluated in different phosphate-buffered saline (PBS) solutions (pH 5.0 and pH 7.4). As shown in Fig. 4, cumulative release of DOX from TiO_2–PEG–DOX NPs was about 50% at pH = 7.4, which was close to the pH of physiological blood. However, around 80% of DOX was released at pH = 5.0, which imitated the pH value of tumors. The results indicated that the TiO_2–PEG–DOX NP is a smart controlled release system, and could release DOX more specifically and effectively in an acidic tumor environment, which is favorable for the controlled release and targeted chemotherapy and reducing its systemic toxicity *in vivo*. Therefore, PEG coating not only improved the stability of TiO_2–PEG NPs, but also attenuated the interactions between the two components which boosted the drug release in an acidic environment compared with our previous work.[26]

The cellular uptake and intracellular distribution of DOX were observed under a confocal laser scanning microscope, and the data showed a time dependent cellular uptake for both free DOX and TiO_2–PEG–DOX NPs. In the free DOX treatment group, most of the drug was located uniformly with Hoechst, which indicated that the free DOX was accumulated in the nuclei of MDA-MB-231-GFP-fLuc cells at 2 h (Fig. 5i–l). When the incubation time was prolonged from 2 h to 4 h, more DOX was concentrated in the nuclei of cells (Fig. 5m–p). However, in the TiO_2–PEG–DOX NP treatment group, DOX was initially localized in the cytoplasm after 2 h incubation

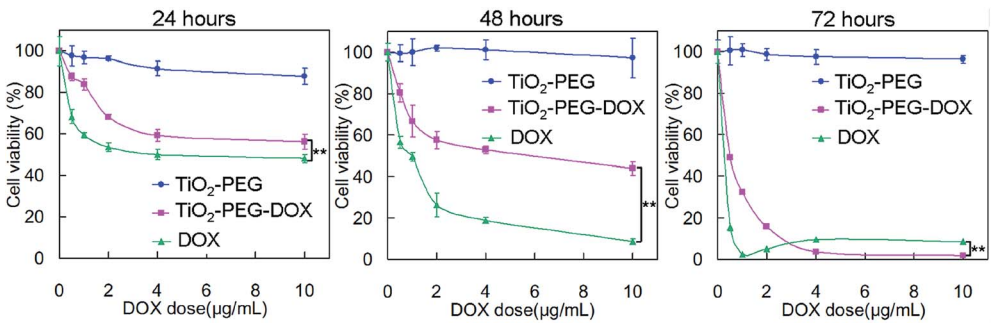

Fig. 6 Cell viability assay of MDA-MB-231-GFP-fLuc cells with different treatments for 24, 48 and 72 h, respectively (** $P < 0.01$).

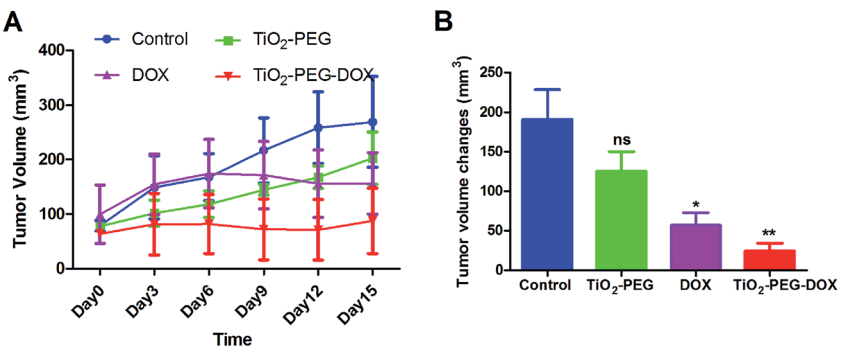

Fig. 7 The tumor volume changes after different treatments for continuous 15 days. The average tumor volume (A) and tumor volume changes (B) treated with control, TiO_2–PEG, DOX and TiO_2–PEG–DOX NPs. The average tumor volume changes are presented as tumor $volume_{day15}$ − tumor $volume_{day0}$ (ns $P > 0.05$, * $P < 0.05$, ** $P < 0.01$).

(Fig. 5q–t), because NPs were mainly distributed in the endosomes after taken up by the cells. While DOX was transported to the nuclei after 4 h incubation with TiO_2–PEG–DOX NPs, which suggested that the release of DOX from the NPs was prolonged in the acidic endosomes (Fig. 5u–x).

We further investigated the antitumor cell effects of free DOX or TiO_2–PEG–DOX NPs on MDA-MB-231-GFP-fLuc breast cancer cells *in vitro*. As shown in Fig. 6, the cell viability of cancer cells treated with free DOX or TiO_2–PEG–DOX NPs both significantly decreased compared to the treatment of TiO_2–PEG NPs. At 24 and 48 h, free DOX exhibited stronger cytotoxicity compared to the TiO_2–PEG–DOX NP treatment. Around 91.22 ± 1.02% of cells were killed at 48 h during 10 μg mL^{-1} of free DOX treatment. However, only 56.24 ± 3.32% cancer cells were killed in the TiO_2–PEG–DOX NP treatment group at 48 h. At 72 h, 91.42 ± 0.31% of cells were killed in free DOX treatment, while 98.08 ± 0.29% cells were killed in TiO_2–PEG–DOX NP treatment. The data suggested that TiO_2–PEG–DOX NPs possessed prolonged drug release and higher antitumor cell capabilities. Taken together, these *in vitro* studies demonstrated that the antitumor efficacy of DOX was enhanced upon loading onto TiO_2–PEG nanocarriers.

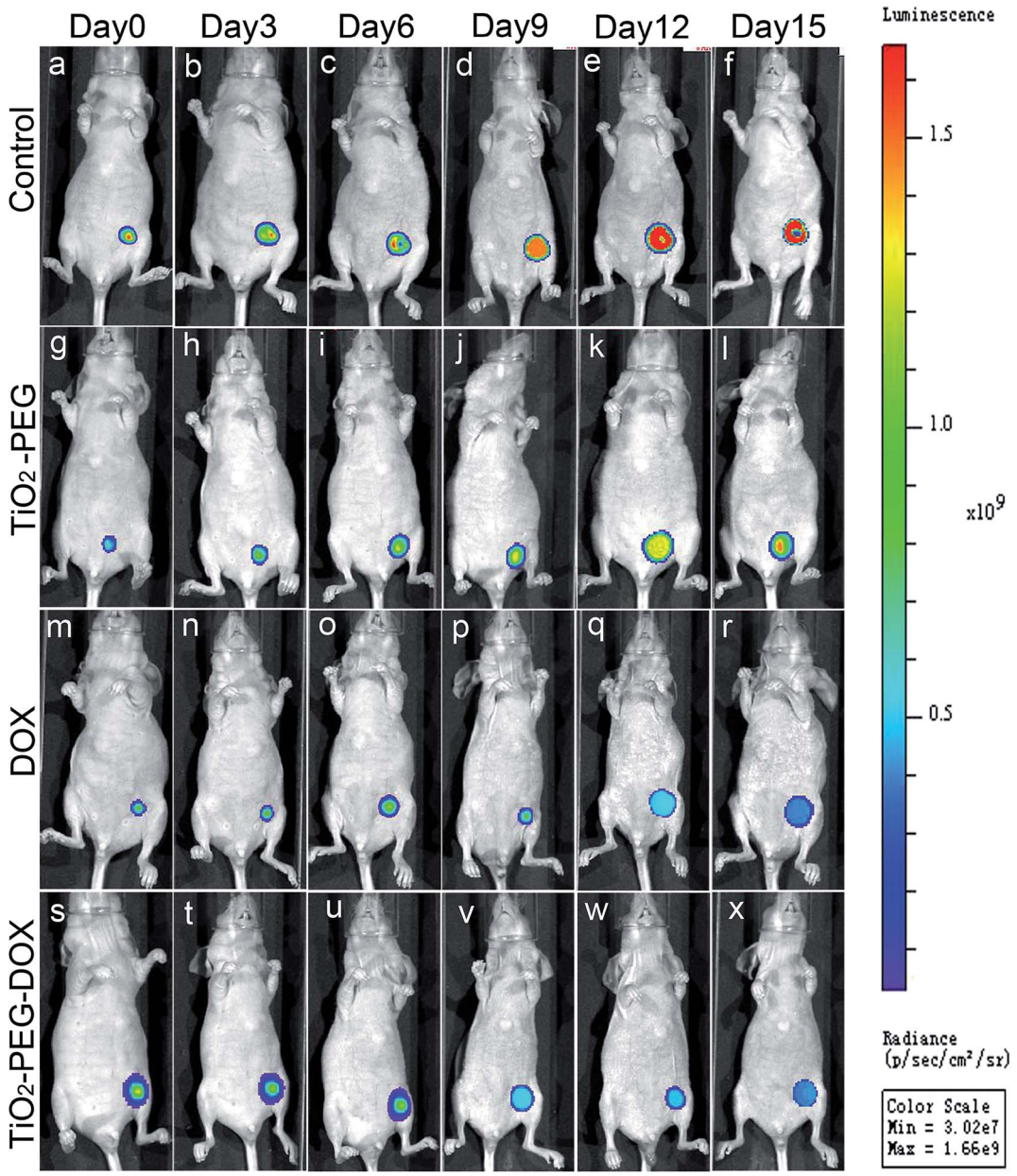

Fig. 8 The representative BLI of tumors *in vivo* with different treatments for continuous 15 days. With the aid of labeled fLuc, the nude mice bearing breast tumors derived from MDA-MB-231-GFP-fLuc cells displayed BLI, the signal intensities of which reflected the tumor growth conditions and drug treatment efficacy *in vivo*. The BLI of breast tumors with different treatments included control group (a–f), TiO_2–PEG treatment (g–l), DOX treatment (m–r), and TiO_2–PEG–DOX treatment (s–x).

3.3 *In vivo* evaluation of tumor growth with different drug treatments

In this study, we proceeded to evaluate the antitumor treatment efficacy of TiO_2–PEG–DOX NPs *in vivo* in an orthotopic breast tumor-bearing mouse model, because it is a preferable animal model for simulating tumor development in human beings. To compare the therapeutic effects in different drug treatment groups, the tumor volumes were initially measured by using a digital caliper every 3 days, and the tumor volume changes were calculated and presented as tumor $volume_{day15}$ − tumor $volume_{day0}$. The results showed that the tumor volume growth steadily increased for 15 days in the control and TiO_2–PEG NP treatment groups, and the tumor volume changes were 190.90 ± 74.64 mm^3 and 125.0 ± 50.36 mm^3, respectively. In the DOX treatment group, the tumor volume increased during the initial 6 days and then gradually decreased thereafter, and the tumor volume change was 56.19 ± 31.85 mm^3 after 15 days. While TiO_2–PEG–DOX NP treatment significantly inhibited the tumor volume growth during the whole 15 day period, and the tumor volume change was only 24.10 ± 19.62 mm^3. The above data suggested that TiO_2–PEG nanocarriers facilitated the antitumor efficacy of DOX *in vivo* (Fig. 7).

It is known that optical molecular imaging such as bioluminescence imaging (BLI) was sensitive and accurate for the detection and monitoring of tumor growth compared to the traditional manual measurement. Because the BLI signal was derived from living tumor cells, it provided a quantitative surrogate measurement and reflected the number of living tumor cells. Therefore, in this study, the antitumor therapeutic efficacy was also examined dynamically by using BLI besides measuring tumor volumes using digital calipers. With the aid of fLuc labeled MDA-MB-231-GFP-fLuc cancer cells, the nude mice bearing orthotopic breast tumors displayed a strong BLI signal in the tumor regions. The BLI imaging of breast tumor bearing mice with different treatments is shown in Fig. 8. The BLI light intensity kept increasing in the control and TiO_2–PEG NP treatment groups during the whole 15 day observation. In the free DOX treatment group, the BLI light intensity increased during the initial 6 day treatment, and then gradually decreased. The BLI intensity was maintained at a relatively low level in the TiO_2–PEG–DOX NP treated group suggesting a better tumor growth suppression effect compared with other treatment groups. The BLI intensity values of the control group and the TiO_2–PEG NP group were 8.99 ± 2.06 × 10^9 and 7.55 ± 1.82 × 10^9 photons per s per cm^2 at day 15. The BLI intensity of the free DOX group was 1.77 ± 1.38 × 10^9 photons per s per cm^2 at day 15, while the TiO_2–PEG–DOX NP treatment group was only 1.00 ± 1.05 × 10^9 photons per s per cm^2 (* $P < 0.05$, ** $P < 0.01$) (Fig. 9). The BLI data, consistent with the manual caliper measurement, demonstrated TiO_2–PEG–DOX NPs exhibiting enhanced antitumor activity over free DOX in terms of tumor growth suppression.

To further confirm the *in vivo* tumor inhibition effects, tumor nodules were dissected out at the end of drug treatment and histological HE staining and CD31 immunofluorescence staining were performed. For the HE staining, the cell nucleus

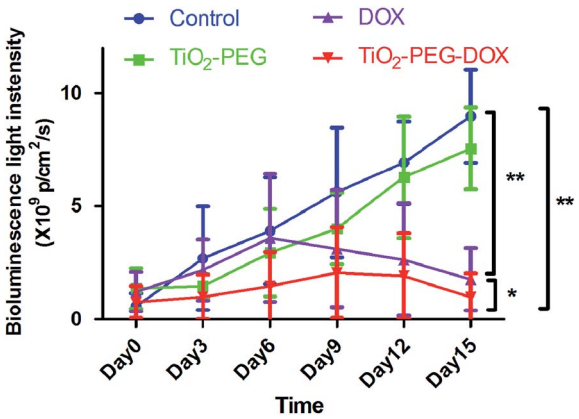

Fig. 9 Bioluminescent light (BLI) intensities of tumors in the control, TiO_2–PEG, DOX and TiO_2–PEG–DOX groups (* $P < 0.05$, ** $P < 0.01$).

was stained blue by hematoxylin, and the cytoplasm was stained pink by eosin. The necrotic cells did not have a clear cell morphology and the nuclei became pyknotic or absent. The HE staining results showed that the tumor size and tumor cell number decreased in the DOX and TiO_2–PEG–DOX NP treatment groups compared to the control and TiO_2–PEG NP groups. Moreover, there were more necrotic cells found inside tumors in TiO_2–PEG–DOX treatment compared to the DOX treatment, but not in the control and TiO_2–PEG NP groups (Fig. 10a–d).

The microvascular marker CD31 immunostaining results showed that CD31 expression decreased in the DOX and TiO_2–PEG–DOX NP treated tumors compared to the control and TiO_2–PEG NP treated tumors (Fig. 10e–h, arrows). In addition, there was more red fluorescence of DOX detected in the TiO_2–PEG–DOX NP group than in the free DOX treated tumors (Fig. 10i–l, arrows). The results indicated that TiO_2–PEG nanocarriers can facilitate the infiltration of DOX in tumor regions, which can increase the antitumor and antiangiogenesis efficacy. The nuclei were stained using DAPI (Fig. 10m–p), and the merged images of CD31, DOX and DAPI are also presented (Fig. 10q–t).

Based on the above experiments, the data altogether manifested that TiO_2–PEG–DOX NPs possessed improved antitumor efficacy compared to the free DOX both *in vivo* and *in vitro*. One reason for the improved antitumor activity might be the enhanced accumulation of the TiO_2–PEG–DOX NPs at the tumor site for the EPR effect. Moreover, the acidic tumor environment facilitating the release of DOX from NPs may also contribute to the therapeutic efficacy.

3.4 Safety assessment of TiO_2–PEG NPs *in vivo*

It is well known that the chemotherapeutic effects of DOX may cause systemic adverse side effects *in vivo*, so we further examined the toxicity of free DOX and TiO_2–PEG–DOX NPs during the whole treatment period. The body weight loss is known to be an important indicator for evaluating drug-related toxicity. After 15 day drug treatment, the mice body weight changes were calculated and presented as body $weight_{day15}$ − body $weight_{day0}$. The data showed that the mice body weight in the control and TiO_2–PEG NP groups steadily increased, and the

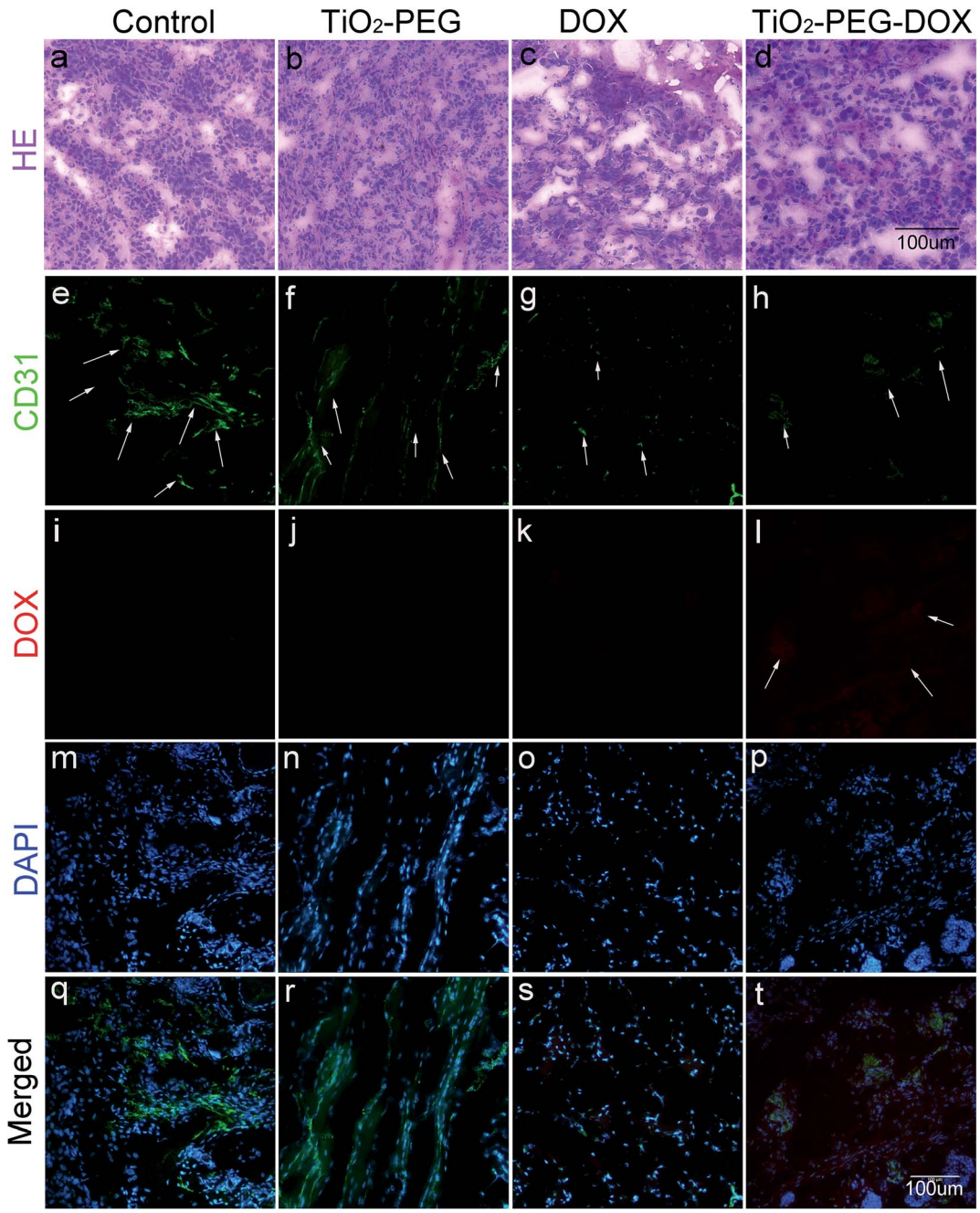

Fig. 10 The histology and CD31 immunofluorescence staining of tumor sections after different treatments for continuous 15 days. HE staining of tumors is shown in (a–d). CD31 is a microvascular marker, and was stained to evaluate the anti-angiogenic effects of different drug treatments. The CD31 expression is shown (e–h, arrows): CD31 expression showing the green color; (i–l, arrows): the red fluorescence of DOX; (m–p) the nuclear staining DAPI showing the blue color; (q–t): merged images of both CD31, DOX and DAPI (scale bar = 100 μm, 20×).

body weight changes were 13.1 ± 1.42 g and 12.93 ± 0.39 g, respectively after 15 day treatment. DOX treatment caused a significant loss of body weight, and the body weight change was −2.5 ± 2.06 g (** $P < 0.01$) (Fig. 11). As for the TiO_2–PEG–DOX NP treatment group, the mice body weight did not exhibit significant changes (−0.24 ± 0.61 g) during the 15 day treatment period. The data indicated that TiO_2–PEG nanocarriers were able to decrease the toxicity of DOX and reduce its systemic side effects *in vivo*.

We further examined the toxicity of the free DOX and TiO_2–PEG–DOX NP treatment to the major organs of the breast tumor bearing mice. The histological HE staining of the liver, kidney and heart was performed and we found hepatotoxicity in the DOX-treated group, but not in the TiO_2–PEG–DOX NP treated group (Fig. 12a–d). In addition, the DOX treatment caused nephrotoxicity, whereas no obvious abnormalities were found in other treatment groups (Fig. 12e–h). There were no abnormalities found in the heart in all treatment groups

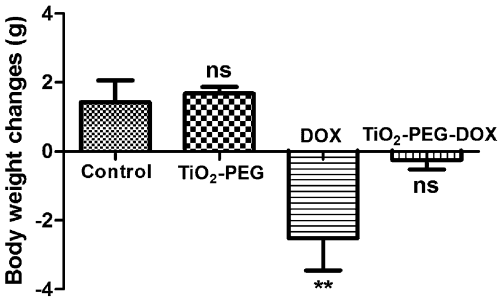

Fig. 11 The mouse body weight changes after different treatments for 15 days. The average body weight changes are presented as body $\text{weight}_{\text{day15}} - \text{body weight}_{\text{day0}}$ (ns $P > 0.05$, ** $P < 0.01$).

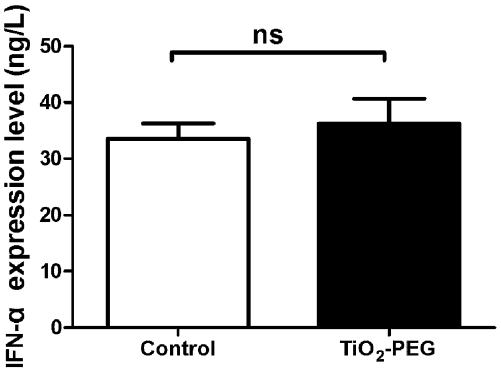

Fig. 13 The early immunogenic response of TiO_2–PEG by measuring the IFN-α level in blood plasma samples (ns $P > 0.05$).

(Fig. 12i–l). The results indicated that the TiO_2–PEG nanocarrier can reduce the systemic toxicity of DOX to the major organs *in vivo*.

Moreover, the safety of the TiO_2–PEG NP itself as an *in vivo* drug delivery carrier is critical for further application, and was evaluated in our study. The early immunogenic response of TiO_2–PEG NPs was monitored by measuring the serum IFN-α level,[34] and the data showed that there was no statistical difference between TiO_2–PEG NP treated and saline treated mice (Fig. 13). The data suggested that the TiO_2–PEG NP can be utilized as a safe drug carrier for *in vivo* application.

4. Conclusion

In summary, our study demonstrated that TiO_2–PEG–DOX nanoparticles, as safe drug carriers, increased the delivery of DOX to the tumor site and displayed enhanced antitumor efficacy *in vivo*. The size of TiO_2–PEG–DOX nanoparticles met the EPR effects of tumors with increased passive drug accumulation in the tumor region, and the nanoparticles possessed a stable hydrated diameter in serum. The *in vitro* cell viability experiment revealed an enhanced and prolonged inhibition of cell proliferation of TiO_2–PEG–DOX nanoparticles compared with free DOX. With the aid of optical molecular imaging, the

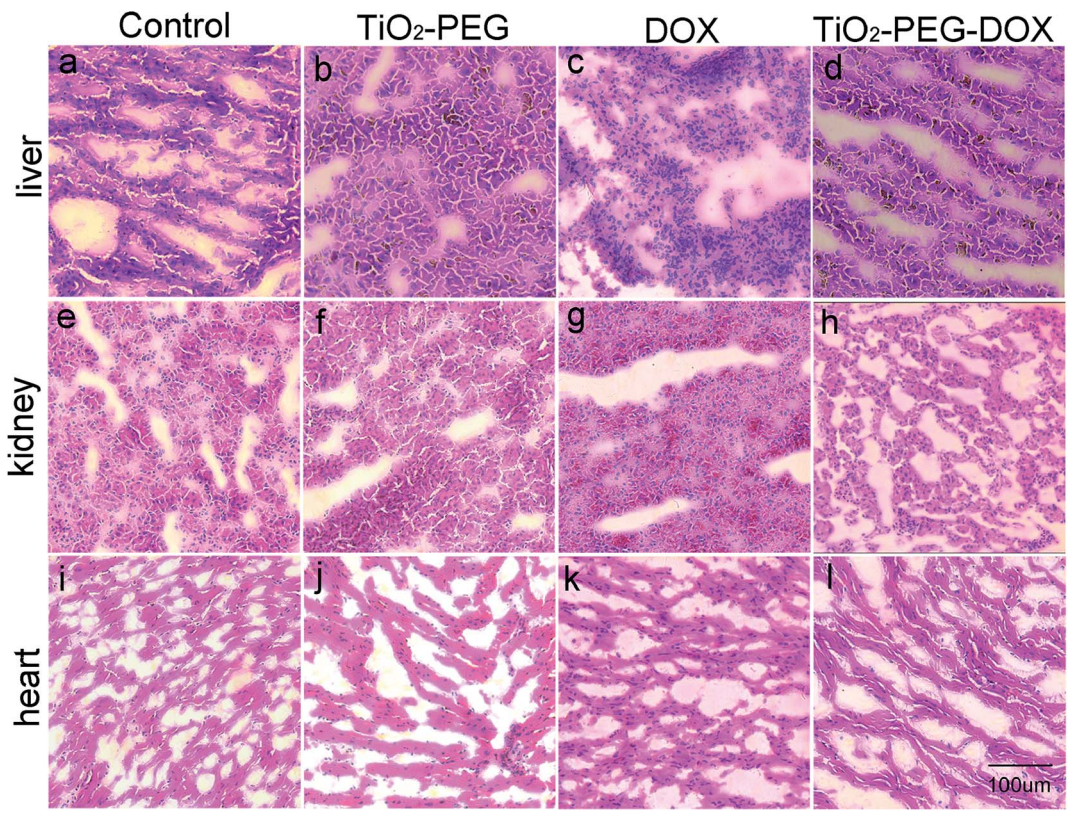

Fig. 12 The histological assessment of major organs including the liver, kidney and heart is shown. The sections were stained with hematoxylin and eosin (HE) before examination *via* light microscopy (scale bar = 100 μm, 20×).

enhanced antitumor efficacy of TiO_2–PEG–DOX NPs was dynamically and noninvasively examined by using BLI on the orthotopic MDA-MB-231-GFP-fLuc breast tumor bearing nude mice. In addition, the improved anticancer efficacy was further validated through histology and CD31 immunostaining of tumor tissues. Furthermore, the TiO_2–PEG NPs were proved to be safe and biocompatible nanocarriers by testing the histology of major organs and the serum immunogenic IFN-α level. Overall, the TiO_2–PEG NPs working as safe and biocompatible nanocarriers *in vivo* can enhance the antitumor efficacy and minimize the systemic adverse side effects of chemotherapeutic drugs *in vivo*. Our work may provide an experimental basis for the potential clinical translation of TiO_2–PEG NPs as an efficient and safe chemotherapeutic agent delivery platform.

Acknowledgements

This work was supported by the National Natural Science Foundation of China (81227901, U1332117, 61231004 and U1432114), the Research and Development Program of China (973) under Grant (2011CB707702, 2014CB748600 and 2015CB755500), the Hundred Talents Program of Chinese Academy of Sciences (2010-735), and the Natural Science Foundation of Ningbo (Grant no. 2014A610166). This work was supported in part by the State Key laboratory of Management and Control for Complex Systems under Grant no. Y3S9021F30.

References

1 C. DeSantis, R. Siegel, P. Bandi and A. Jemal, *CA-Cancer J. Clin.*, 2011, **61**, 408–418.
2 D. R. Youlden, S. M. Cramb, N. A. Dunn, J. M. Muller, C. M. Pyke and P. D. Baade, *Cancer Epidemiol.*, 2012, **36**, 237–248.
3 S. Banerji, K. Cibulskis, C. Rangel-Escareno, K. K. Brown, S. L. Carter, A. M. Frederick, M. S. Lawrence, A. Y. Sivachenko, C. Sougnez, L. Zou, M. L. Cortes, J. C. Fernandez-Lopez, S. Peng, K. G. Ardlie, D. Auclair, V. Bautista-Piña, F. Duke, J. Francis, J. Jung, A. Maffuz-Aziz, R. C. Onofrio, M. Parkin, N. H. Pho, V. Quintanar-Jurado, A. H. Ramos, R. Rebollar-Vega, S. Rodriguez-Cuevas, S. L. Romero-Cordoba, S. E. Schumacher, N. Stransky, K. M. Thompson, L. Uribe-Figueroa, J. Baselga, R. Beroukhim, K. Polyak, D. C. Sgroi, A. L. Richardson, G. Jimenez-Sanchez, E. S. Lander, S. B. Gabriel, L. A. Garraway, T. R. Golub, J. Melendez-Zajgla, A. Toker, G. Getz, A. Hidalgo-Miranda and M. Meyerson, *Nature*, 2012, **486**, 405–409.
4 S. K. Carter and M. Slavik, *Annu. Rev. Pharmacol.*, 1974, **14**, 157–183.
5 B. A. Chabner and T. G. Roberts, *Nat. Rev. Cancer*, 2005, **5**, 65–72.
6 R. Singh and J. W. Jr Lillard, *Exp. Mol. Pathol.*, 2009, **86**, 215–223.
7 K. Cho, X. Wang, S. Nie, Z. G. Chen and D. M. Shin, *Clin. Cancer Res.*, 2008, **14**, 1310–1316.
8 D. Peer, J. M. Karp, S. Hong, O. C. Farokhzad, R. Margalit and R. Langer, *Nat. Nanotechnol.*, 2007, **2**, 751–760.
9 K. Greish, *Cancer Nanotechnology*, Springer, 2010. pp. 25–37.
10 Y. Matsumura and H. Maeda, *Cancer Res.*, 1986, **46**, 6387–6392.
11 E. S. Lee, Z. Gao and Y. H. Bae, *J. Controlled Release*, 2008, **132**, 164–170.
12 S. Bhattacharyya, R. A. Kudgus, R. Bhattacharya and P. Mukherjee, *Pharm. Res.*, 2011, **28**, 237–259.
13 F. M. Kievit, F. Y. Wang, C. Fang, H. Mok, K. Wang, J. R. Silber, R. G. Ellenbogen and M. Zhang, *J. Controlled Release*, 2011, **152**, 76–83.
14 H. Meng, M. Liong, T. Xia, Z. Li, Z. Ji, J. I. Zink and A. E. Nel, *ACS Nano*, 2010, **4**, 4539–4550.
15 J. Wu, Y. Wang, X. Yang, Y. Liu, J. Yang, R. Yang and N. Zhang, *Nanotechnology*, 2012, **23**, 355101.
16 H. C. Arora, M. P. Jensen, Y. Yuan, A. Wu, S. Vogt, T. Paunesku and G. E. Woloschak, *Cancer Res.*, 2012, **72**, 769–778.
17 P. K. Jain, X. Huang, I. H. El-Sayed and M. A. El-Sayed, *Acc. Chem. Res.*, 2008, **41**, 1578–1586.
18 V. Biju, T. Itoh, A. Anas, A. Sujith and M. Ishikawa, *Anal. Bioanal. Chem.*, 2008, **391**, 2469–2495.
19 S. Yamaguchi, H. Kobayashi, T. Narita, K. Kanehira, S. Sonezaki, Y. Kubota, S. Terasaka and K. Houkin, *Ultrason. Sonochem.*, 2010, **86**, 964–971.
20 H. Zhang, C. Wang, B. Chen and X. Wang, *Int. J. Nanomed.*, 2012, **7**, 235–242.
21 M. Song, R. Zhang, Y. Dai, F. Gao, H. Chi, G. Lv, B. Chen and X. Wang, *Biomaterials*, 2006, **27**, 4230–4238.
22 B. Wang, E. Yantsen, T. Larson, A. B. Karpiouk, S. Sethuraman, J. L. Su, K. Sokolov and S. Y. Emelianov, *Nano Lett.*, 2009, **9**, 2212–2217.
23 Y. Harada, K. Ogawa, Y. Irie, H. Endo, L. B. Feril Jr, T. Uemura and K. Tachibana, *J. Controlled Release*, 2011, **149**, 190–195.
24 S. Shen, X. Guo, L. Wu, M. Wang, X. Wang, F. Kong, H. Shen, M. Xie, Y. Ge and Y. Jin, *J. Mater. Chem. B*, 2014, **2**, 5775–5784.
25 Y. Chen, Y. Wan, Y. Wang, H. Zhang and Z. Jiao, *Int. J. Nanomed.*, 2011, **6**, 2321–2326.
26 W. Ren, L. Zeng, Z. Shen, L. Xiang, A. Gong, J. Zhang, C. Mao, A. Li, T. Paunesku, G. E. Woloschak, N. S. Hosmaned and A. Wu, *RSC Adv.*, 2013, **3**, 20855–20861.
27 D. Peer, J. M. Karp, S. P. Hong, O. C. Farokhzad, R. Margalit and R. Langer, *Nat. Nanotechnol.*, 2007, **2**, 751–760.
28 K. Cho, X. Wang, S. Nie, Z. Chen and D. M. Shin, *Clin. Cancer Res.*, 2008, **14**, 1310–1316.
29 S. D. Perrault, C. Walkey, T. Jennings, H. C. Fischer and W. C. Chan, *Nano Lett.*, 2009, **9**, 1909–1915.
30 R. Weissleder, *Science*, 2006, **312**, 1168–1171.
31 R. Weissleder and M. J. Pittet, *Nature*, 2008, **452**, 580–589.
32 Q. Yuan, W. A. Yeudall and H. Yang, *Biomacromolecules*, 2010, **11**, 1940–1947.
33 S. Aryal, C. M. Hu and L. Zhang, *ACS Nano*, 2010, **4**, 251–258.
34 H. Lee, A. K. Lytton-Jean, Y. Chen, K. T. Love, A. I. Park, E. D. Karagiannis, A. Sehgal, W. Querbes, C. S. Zurenko, M. Jayaraman, C. G. Peng, K. Charisse, A. Borodovsky, M. Manoharan, J. S. Donahoe, J. Truelove, M. Nahrendorf, R. Langer and D. G. Anderson, *Nat. Nanotechnol.*, 2012, **7**, 389–393.